THE IMPLICATIONS OF FLOW STRUCTURES IN BLOOD FLOW IN HEALTHY AND UNHEALTHY AORTA

Yuxi Jia[1 *], Chris Aitken[1], Arman Hemmati[1 ¥], Kumaradevan Punithkumar[2 3], Michelle Noga[3]

[1] Department of Mechanical Engineering, University of Alberta, Edmonton, AB, Canada
[2] Department of Electrical Engineering, University of Alberta, Edmonton, AB, Canada
[3] Department of Diagnostic Imaging & Radiology, University of Alberta, Edmonton, AB, Canada

ABSTRACT

The blood flow through a healthy and unhealthy aorta is simulated using Fluid-Structure-Interaction in OpenFOAM based on patient specific characteristics. The aorta geometry is obtained from Magnetic Resonance Imaging (MRI), which are modelled as deformable arterial walls to simulate the blood flow. The pressure and velocity profiles display similar trends in both aortas, although the unhealthy aorta shows lower velocity magnitudes and a higher systolic and diastolic blood pressure using identical inlet conditions. Without having an increased radius, the reduction on blood flow velocity in the unhealthy aorta suggests a decrease in blood circulation. To compensate for the decreased blood flow rate, an increased inlet blood velocity may be required for the unhealthy aorta, resulting in an elevated risk of high blood pressure.

INTRODUCTION

Cardiovascular disseases are the leading cause of death globally, with high blood pressure being the most frequent cause of death (NIH, 2018). The reconstruction of large blood vessels, including the aorta, is a difficult surgical task in pediatric cardiology. Of those receiving aortic or pulmonary artery reconstruction, 20% require re-operation or intervention at a later date (Vitanova et al., 2017). This research aims to improve surgical outcomes for aortic and pulmonary artery reconstruction by personalizing surgical operations, which brings benefit to patients and the health care system.

The study of blood flow has been the subject of several investigations over the years (Liu et al., 2011 and Crosetto et al., 2011). A variety of conditions are commonly varied based on the desired outcomes of the research. Common considerations include: Newtonian and Non-Newtonian (Johnston et al., 2004), steady and pulsatile flow (Armstrong et al., 2019), turbulence model (Song et al., 2003), rigid and deformable walls (Crosetto et al., 2011), and boundary conditions (Vita et al., 2015). The variations of these parameters alters simulation results, by changing the wall shear stress, velocity and pressure fields and mass transport.

There is a large influence of Fluid-Structure-Interaction (FSI) on the distribution of velocity and pressure, which require utilizing compliable aorta walls. The use of rigid arterial walls generally underestimates the flow velocity, and overesimates the blood pressure, while also affecting the distribution of velocity and pressure throughout the aorta (Maivè et al., 2012). The periodic blood flow rate, undergoing systole and diastole, also significantly impacts the velocity and pressure within the aorta at different stages of the pulsation flow, and is required for obtaining physical results (Armstong et al., 2018).

The transient nature of blood flow through the cardiac cycle requires unsteady modeling of the flow. These models provide the periodic pressure data that is valuable in interpretation of patient-specific systolic and diastolic pressure (Olusen et al., 2000). These results are critical in investigating the gravity of cardiovascular diseases, due to the severity of high blood pressure (Chobanian et al., 2003).

The transition to turbulence is a preferred outcome that is expected medically to occur in the aorta since it causes clot formation. However, the flow in the aorta cannot be assumed to be fully laminar, since anomolies may lead to small size eddy formations that are treated as turbulent effects. These are the potential observations of cardiovascular disorder. Many previous studies have used laminar models, as the accuracy of simple turbulence models including Reynold's Averaged Navier-Stokes (RANS) k-ε and k-ω have shown poor results (Zhang et al., 2013). Thus, it is recommended to utilize a direct approach in simulating the flow.

According to Doost et al, 2016, the non-Newtonian characteristics are negligible if the artery size is greater than 2 mm. Thus, since the aorta diameter is greater than 2 mm, blood can be simulated as a Newtonian fluid. Although the Newtonian fluid model cannot capture all the effects of blood rheology, it provides a reasonally accurate solution to capture main characteristics of the flow while avoiding the high computational cost of simulating platelet-platelet interactions individually (Khan et al., 2016). The results of many previous simulations have been validated with experimental observations to convey physical understanding of blood flow phenomenon. Long et al. (2005) determined that the difference in viscoelasticity of paediatric blood and adult blood are not significant, so strain properties of adult blood may be applied directly for paediatric studies. Crosetto et al. (2005) showed the shortcomings of rigid wall assumptions, failing to predict essential blood flow characteristics, such as wave pressure propagation. Olusen et al. (2000) performed pressure profile comparisons between experimental and simulation results, validating the ability of blood flow simulations to adequately predict the blood pressure throughout a periodic cycle.

This study is a subset of a larger research initiative that aims to build patient-specific templates for aortas of various geometries to synchernize surgical procedures. This is pursued by performing computational fluid dynamics simulations to identify optimized blood flow characteristics that control pressure drop and blood flow rate for different aorta geometries prior to surgery. The current study emplys patient-specific healthy and unhealthy aorta models using individualized boundary conditions to simulate flow abnormalities in the unhealthy aorta. The unhealthy aorta model will be modified to best resolve significant flow abnormalities, aimed at minimizing physical modifications of the aorta.

* yjia2@ualberta.ca
¥ arman.hemmati@ualberta.ca

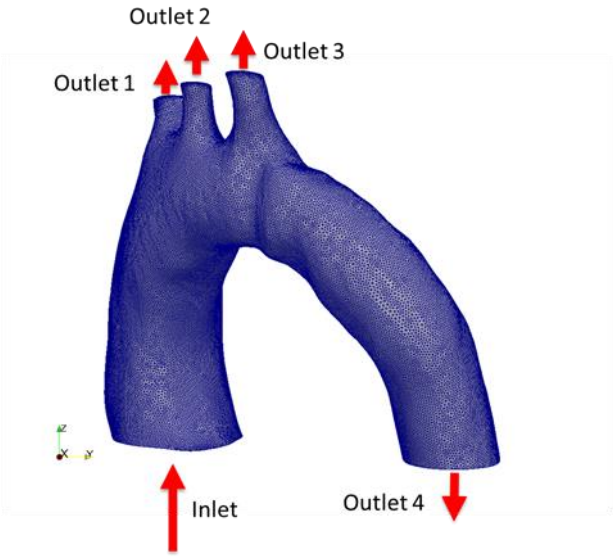

Figure 1: Mesh of Healthy Aorta

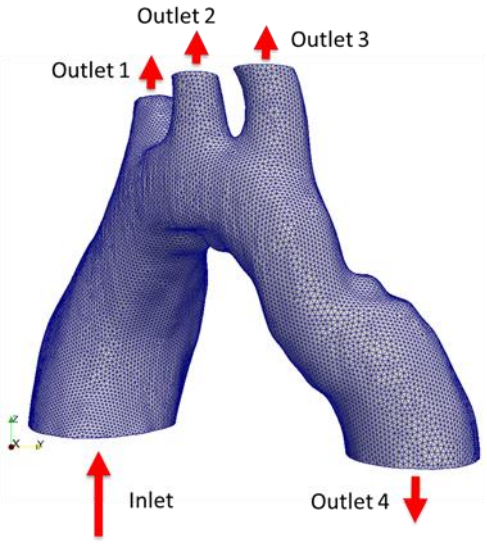

Figure 2: Mesh of Unhealthy Aorta

METHODOLOGY

The blood flow through two aorta geometries (healthy and unhealthy cases) are simulated directly using the FSI module in OpenFOAM, which is an open source computational fluid dynamics software. Particularly, *extend-foam-4.0* is used to implement the fsiFoam solver, which is an extension to OpenFOAM.

Complex geometries of patient-specific MRI and Computerized Tomography (CT) models were used to study the differences in blood flow for healthy and unhealthy aortas. The complex models used in this study were segmented from CT scans using Simpleware ScanIP. Using the attained fluid model boundaries, compliable aorta walls were created for the simulations.

The unhealthy aorta used in this investigation is from a patient with a bicuspid aortic valve (BAV) and a coarctation of the aorta. A BAV increases the likelihood of developing aortic stenosis and aortic regurgitation. The heart becomes less effective at preventing backflow during diastole, requiring higher blood flow during systole to compensate. This requires higher blood pressure through the left ventricle and aorta, and increases the risk of hypertension (Ward, 2000). The aortic narrowing is most common in the aortic arch during aortic coarctation. Since the aorta is narrowed, the left ventricle must generate a higher blood pressure to maintain healthy blood flow. High blood pressure is common in patients with coarctation of the aorta, and continues to be common and potentially serious in patients who have undergone anatomically successful repair (Liberthson et al., 1979 and Canniffe et al., 2013).

An in-homogeneous grid was structured using a total of 4.0×10^6 tetrahedral elements, with a fine prism layer surrounding the boundaries of the fluid domain to ensure adequate grid spacing at the boundary layer. The inlet conditions were selected to be identical for the two cases, with a uniform pressure and a fully developed velocity profile following the work of Alastruey et al (2016). Patient-specific velocity data was captured along several planes using MRI at various times during the cardiac cycle, and is used as the velocity inlet condition. The walls of the aorta were assigned a no slip boundary condition and the outlets of both healthy and unhealthy aortas have pressure outlet condition with varying uniform pressure following the work of Vignon-Clementel et al. (2006). The boundary pressure is highest at the inlet, and decreases for each outlet farther down the aorta. The inlets and outlets of the aorta are labelled for the healthy and unhealthy cases in Figures 1 and 2, respectively.

This study assumes blood acts as a Newtonian fluid since several studies have revealed that non-Newtonian characteristics do not affect capturing main flow features in blood vessels with a diameter larger than 2 mm (Doost et al., 2016). Although blood is known to have shear thinning properties, the shear rate of blood near the boundaries of the aorta are expected to be sufficiently low that shear thinning does not dominate the flow. Since the aorta is the only blood vessel in the body where transition to turbulence may occur in unhealthy cases due to high velocities (Stein, PD and Sabbah, HN, 1976), and simple turbulence models such as RANS k-ε fail to accuracy portray key flow characteristics, we chose to directly solve the flow equations. All pressure and velocity results are normalized by the initial inlet pressure and velocity conditions. All length parameters are normalized by the diameter of the corresponding aorta inlet.

The pulsatile nature of blood is modelled using a standard heart rate of 80 beats per minute following Vitanova et al. (2017). The systolic and diastolic cycles were approximated using an idealized pulsated flow waveform following the work of Vita et al. (2015), and it is implemented using four piecewise polynomial functions with two regions of zero magnitude. In Figure 3, he period found between 0.1s and 0.45s represents the systolic cycle of the heart, while the remaining time between 0.45s and 0.1s of the next period represents the diastolic cycle. The focus of our investigation is on results of velocity and pressure profiles at 15s and 25s since they are two regions of interest in medical applications. The former represents the time of zero inlet velocity, and the latter reflects the instance and shortly after the time of maximum inlet velocity.

Two unique characteristics of this study compared to previous simulations of the aorta are: (1) accounting for the FSI between blood and the aorta walls on blood flow characteristics by making the aorta walls compliable, (2) optimizing the boundary conditions by obtaining patient specific inlet and outlet data, and (3) understanding the flow physics due to aorta anomalies that results in paediatric cardiovascular diseases. The interactions between the blood and the aorta walls were captured using Gauss-Seidel iteration scheme. The convergence

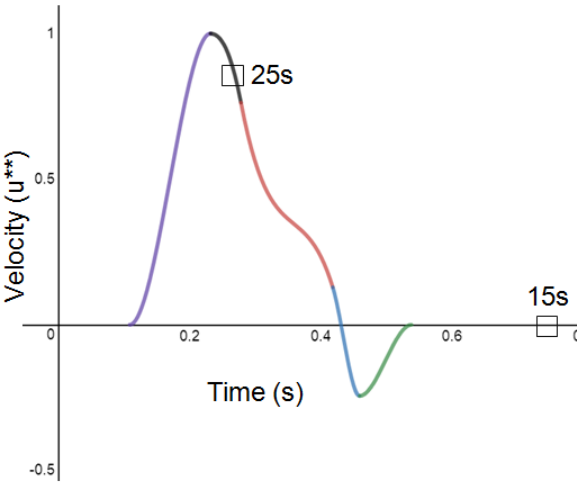

Figure 3: Transient Flow Waveform. Here, u** is defined as velocity normalized by the maximum velocity.

is accelerated by the Aitken relaxation or by the interface quasi-Newtonian procedure (Tukovic et al, 2014). The accurate simulation of the interaction of the blood flow and the aorta walls is critical in proper characterization of the flow, particularly in capturing the correct wall shear stresses and the pressure field (Lantz et al., 2011). Meanwhile, the application of real-time patient data on the boundary conditions allows for realistic flow characterization compared to the uniform or parabolic conditions that are typically used for these models (Razavi et al., 2011). This enables a physical interpretation of the aorta anomalies on flow characteristics and means to address them objectively with minor intrusions.

RESULTS

The cross-sectional velocity profiles in **Error! Reference source not found.** displays the velocity in the regions of interest in the aorta with medical implications. That is regions prior to each of the 4 outlets (B, C, D and E) and prior to the branching off of the first outlet (A). The velocities found at A, B, C, and D show similar trends in both aortas at 15s and 25s. In regions A, C, and D, the velocity throughout the entire area is relatively uniform, while in region B, the velocity is maximum near the top of the cross-section, and decreases linearly towards the bottom of the cross-section. There is a discrepancy between the results at E between the two cases that hint at the specific implications associated with anomalies in aortas. In the unhealthy aorta, the velocity at E is relatively uniform, and it has the maximum velocity of the five considered regions at both 15s and 25s. In the case of the healthy aorta, the highest velocity away from the aortic arch is observed at E, and the velocity decreases significantly as it approaches the side proximal to the aortic arch. The highest velocity during diastole at 15s occurs at E, while the maximum velocity during systole at 25s occurs at A.

The velocity streamlines in Figure 5 are obtained by tracing the streamlines through the midplane of the aorta inlet for both the healthy and unhealthy aorta. From the streamlines, it can be observed that maximum velocity in the unhealthy aorta is lower than that of the healthy aorta. Moreover, the average magnitude of velocity in the unhealthy aorta tends to be lower. The flow patterns are similar for both cases, with the maximm velocities generally appearing in the ascending aorta, aortic arch, and descending aorta regions. However, the velocities exiting through the first three outlets tend to be lower. The streamlines

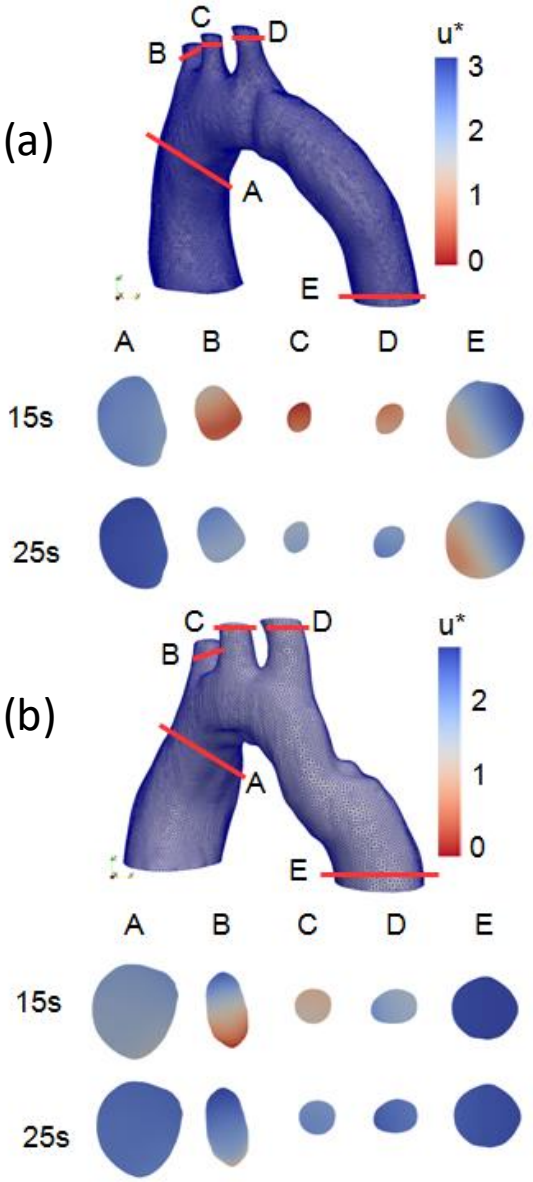

Figure 4: Cross-Sectional Velocity Before Outlets. (a) Healthy Aorta, and (b) Unhealthy Aorta

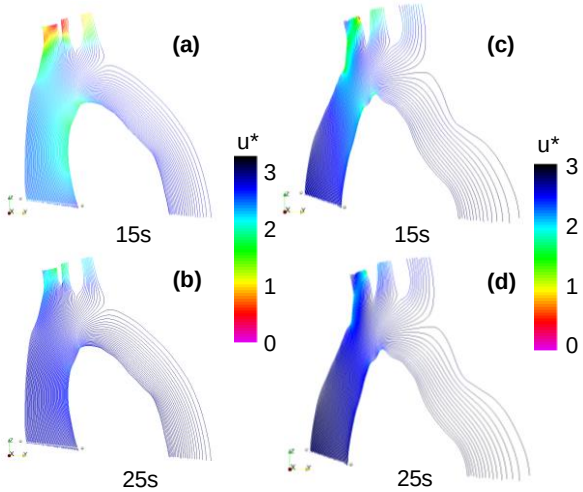

Figure 5: Velocity Streamlines: (a), (b) Healthy Aorta, and (c), (d) Unhealthy Aorta

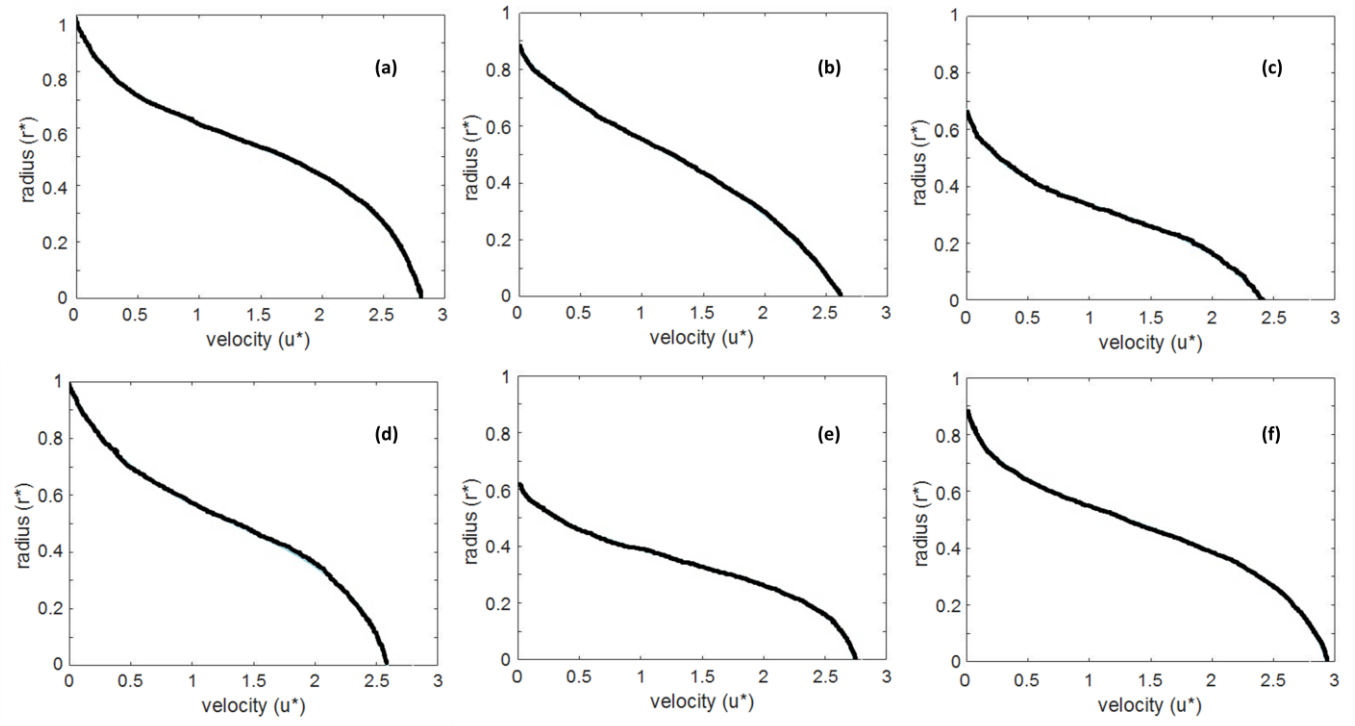

Figure 6: Velocity Profile at 25s: (a) - (c) Healthy Aorta, and (d) - (f) Unhealthy Aorta

coincide closely with the velocity contours in Figure 4, showing that the velocities at 25s is considerably larger than the velocities at 15s, particularly through the first three outlets. The relative velocity magnitudes throughout the two aorta models are generally consistent. However, the velocity through the third outlet of the unhealthy aorta is considebly higher relative to the velocity exiting the third outlet of the healthy aorta. These streamline and velocity contours agree with the results from the previous work of Soudah et al (2017). Soudah's streamline results in Figure 6.1 are similar to the results presented in this study, with the highest velocity in the healthy aorta found in the ascending aorta and small sections of the descending aorta. However, the velocity in the unhealthy aorta is highest in the ascending aorta and also in the majority of the descending aorta.

The velocity profile was obtained at three cross-sections along the aorta at 25s. The plots in **Error! Reference source not found.** display the normalized velocity along the radius of the aorta. The three cros-sectional areas are selected according to their distance along the aorta from the inlet, measuring up through the ascending aorta, through the aortic arch to the descending aorta. In **Error! Reference source not found.**, the inlet is located at z=0, z=2R is 2 radii past the inlet, and z=4R is 4 radii past the inlet (here, R is the radius of the inlet of the aorta). For both the healthy and unhealthy aortas, the cross-section at z=2R coincides with the start of the aortic arch region. However, the z=4R is at the start of the descending aorta. **Error! Reference source not found.** reveals that the velocity profile in each of the 6 cross-sections show the same trend, which can be explained physically as a fully developed flow profile that is affected by a weak flow separation. The values for the normalized radius show that the radius of the healthy aorta decreases from the inlet to the aortic arch, and it continues to decrease at the descending aorta. In contrast, the radius of the aortic arch at z=2R decreases considerably in the unhealthy case, while the radius begins to increase again at the descending aorta. This constitues the main anomoly in the unhealthy aorta. The normalized velocity values in the healthy aorta show that the maximum velocity decreases slightly in the aorch arch compared to the inlet. It decreases more as the flow travels further into the descending aorta. The velocity in the unhealthy aorta shows the opposite trend caused by the anomaly, in which case the maximum velocity increases slightly in the aortic arch region and even more as the flow travels into the descending aorta. The velocity profiles are similar to the previous results from Razavi et al (2011). The profiles at z=2R and z=4R clearly show similar trends as the velocity profiles in Figure 7 of Razavi's simulations at 0.1s. At this instance, Razavi's velocity profile at the inlet is that of a fully developed flow profile undergoing no flow separation, and it is different from the results obtained here. This discrepancy is due to the differences with Razavi's setups, where the fully developed flow profile was imposed on the inlet since it was the best possible boundary condition available for that simulation. However, this boundary condition is not physical, since flow separation should already be present in the flow entering the aorta since the blood flow does not physically begin in the aorta. Thus, blood should have experienced flow separation already from flowing through the heart and prior to reaching the aorta. In contrast, the inlet flow profile showing flow seperation obtained from our simulation is more physical, because it is obtained from patient-specific measurements that has already been subject to the effects of flow separation.

The pressure profile was obtained using the average pressure at a cross-section in the middle of the aortic arch by measuring the pressure throughout a full period starting at 15.1s, which coincides with the beginning of the systolic cycle. This is consistent with previous experiments by Olusen et at (2000), in which he shows in Figure 5 of his work that the pressure profile at various locations throughout the aorta

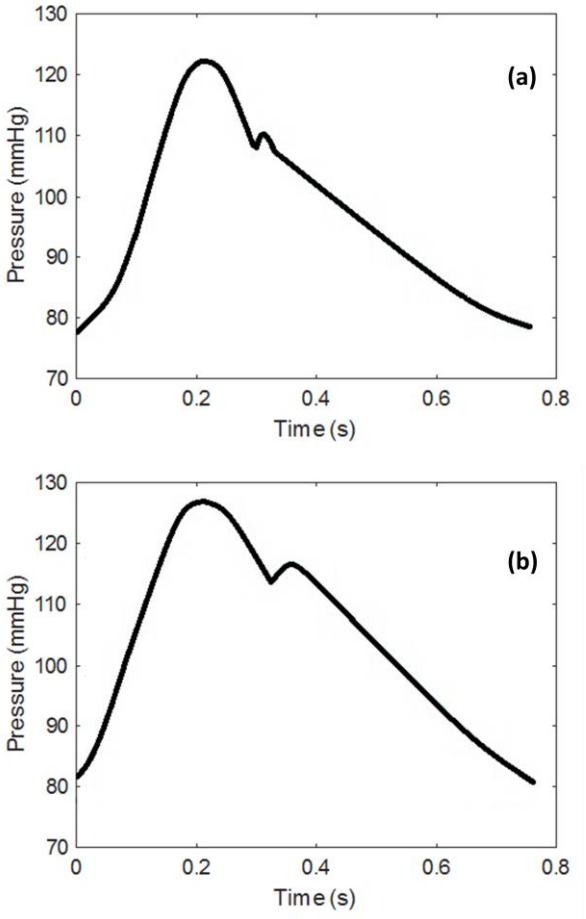

Figure 7: Pressure Profile at 15.1s: (a) Healthy Aorta, and (b) Unhealthy Aorta

remains consistent. The pressure profiles obtained from these simulations show similar trends to the experimental measurements obtained from Olusen et at (2000). However, the simulation profiles are smoother and show less complexities. This is attributed to the idealization of the periodic flow waveform. The pressure profiles from the healthy and unhealthy model are also similar, with the unhealthy pressure profile having a greater maximum and minimum pressure magnitude. Moreover, pressure decreases slower after systole. The maximum pressure during the systolic phase represents the systolic pressure in the pressure profiles, and the minimum pressure occurs during the diastolic phase, which is known as the diastolic pressure. From the healthy aorta, the systolic pressure is ~122 mmHg, while the diastolic pressure is ~77 mmHg. For the unhealthy aorta, the systolic and diastolic pressure are both higher than the healthy aorta, at 127 mmHg and 82 mmHg, respectively. Typically, a systolic and diastolic pressure of 120 mmHg and 80 mmHg is considered to be healthy, and values within 121-139 mmHg and 81-89 mmHg is in the medium risk region (H&SF, 2019). Using these guidelines, the systolic pressure for the healthy aorta is near the lower end of the medium risk region, while the systolic pressure for the unhealthy aorta is near the middle of the medium risk category. The diastolic pressure for the healthy aorta is considered healthy, while the diastolic pressure for the unhealthy aorta is in the medium-risk region.

It is important to note that all comparisons are currently on the basis of healthy and unhealthy aortas having identical boundary conditions. In reality, however, it is unlikely that the inlet velocity profile for the healthy and unhealthy aorta will remain identical. The velocity and pressure trends are unlikely to change significantly using patient-specific parameters obtained from MRI since they are normalized by their corresponding values at the inlet. Nonetheless, a large change in boundary conditions could cause a noticeable deviation in the results of the two cases in relation to one another. One of the key results that has been apparent from all three sets of velocity data is that the velocity in the healthy aorta tends to be higher than the velocity in the unhealthy aorta. The radius of the healthy aorta is generally also larger than the unhealthy aorta. The combination of larger radius and the higher velocities suggest that the blood flow rate through the healthy aorta is greater than the blood flow rate through the unhealthy aorta if the same conditions are set at the boundaries. In order to naturally compensate for this decreased flow rate, the inlet velocity through the unhealthy aorta is likely to be elevated to provide the required blood flow rate to circulate effectively throughout the body. An increase in the inlet velocity will likewise cause an increased velocity throughout the aorta, which is expected to increase pressure distributions. This would negatively influence the already elevated systolic and diastrolic blood pressures of the unhealthy aorta, and it may lead to complications associated with high blood pressure.

The next step in this project is to obtain an understanding of the blood flow velocity and pressure effects associated with the physical abnormalities of the unhealthy aorta. By understanding the impact the of physical alterations of the aorta walls on the flow parameters, the blood flow through the aorta can be corrected to mimic blood flow through a healthy aorta without the need for significant reconstructive surgery. It can also reduce the risk of complications. This will be tested through minor modifications to the model of the unhealthy aorta to investigate the effects of such changes on the blood flow. The outcome of this process aims to decrease the physical modifications that are required to restore flow deformities in the unhealthy aorta, as opposed to current procedures that require significant alterations to the aorta. This is a process that should be repeated on different unhealthy aortas since patient-specific solutions are expected to be different based on varying aorta deformities resulting in different abnormal flow characteritics. After this process has been applied to a larger range of unhealthy aorta, that certain patterns may be deduced in order to more quickly reach an understanding on correcting future unhealthy aortas for pediatric patients.

CONCLUSION

The velocity profiles show similar trends in general along the aorta in case of both healthy and unhealthy patients. However, the velocities in the unhealthy aorta tend to be lower than that of the healthy aorta. There are slight discrepancies in the aortic arch, where the velocity increases in the unhealthy aorta, but decreases in the healthy aorta. The velocity also has similar trends in relative magnitude in the first (B), second (C), and fourth (E) outlets, while the velocity in the third outlet (D) of the unhealthy aorta is comparatively larger than in the healthy aorta. The decreased velocity in the unhealthy aorta, together with the decreased aorta radius, results in a decreased flow rate, which needs to be compensated through an increased pressure gradient across the aorta.

The pressure profiles in the healthy and unhealthy aorta also show similar trends, although the systolic pressure in the unhealthy aorta takes longer to start its descent potentially due to the decreased velocity causing a delayed effect on pressure. The systolic and diastolic pressures in the healthy aorta were

~122 mmHg and ~77 mmHg, respectively, which is within the range of healthy blood pressure. However, the systolic and diastolic pressures in the unhealthy aorta were at 127 mmHg and 82 mmHg, which are well within the medium risk category. If the inlet velocity of the unhealthy aorta is naturally increased to compensate for the decreased flow rate, the pressure in the aorta would further increase, possibly into the high risk category.

REFERENCES

Alastruey, J., and Xiao, N., and Fok, H., and Schaeffter, T., and Figueroa, C., 2016, "On the impact of modelling assumptions in multi-scale, subject-specific models of aortic haemodynamics", *Journal of the Royal Society Interface*, Vol. 13, Issue 119.

Armstrong, M., and Hroner, J., and Clark, M., and Deegan, M., and Hill, T., and Keith, C., and Mooradian, L., 2018. "Evaluating rheological models for human blood using steady state, transient, and oscillatory shear predictions", *Rheologica Acta*, Vol. 57, pp 705-728.

Canniffe, C., and Ou, P., and Bonnet, D., and Celermajer, D, 2013. "Hypertension after repair of aortic coarctation – A systematic review", *Internation Journal of Cardiology.* Vol. 167, Issue 6, pp 2456-2461.

Chobanian, A., and Bakris, G., and Black, H., 2003. "The Seventh Report of the Joint National Committee on Prevention, Detection, Evaluation and Treatment of High Blood Pressure", *Journal of the American Medical Association.* Vol. 289, Issue 19, pp 2560-2571.

Crosetto, P., and Reymond, P., and Deparis, S., and Kontaxakis, D., and Stergiopulos, N., and Quarteroni, A., 2011, "Fluid-structure interaction simulation of aortic blood flow", *Computers & Fliuds*, Vol. 43, Issue 1, pp 46-57.

Coronary Heart Disease. (n.d.). *National Heart, Lung, and Blood Institute*. Retrieved August 26, 2018.

Doost, S, and Zhong, L., and Su, B., and Morsi, Y., 2016. "The numerical analysis of non-Newtonian blood flow in human patient-specific left ventricle", *Computer Methods and Programs in Biomedicine.* Vol. 127, pp 232-247.

High Blood Pressure. (n.d.). *Heart and Stroke Foundation.* Retrieved May 13, 2019.

Johnston, B., and Johnston., P., and Corney, S., and Kilpatrick, D., 2004. "Non-Newtonian blood flow in human coronary arteries: steady state simulations", *Journal of Biomechanics*. Vol. 37, Issue 5, pp 709-720.

Khan, M., and Steinman, D., and Valen-Sendstad, K., 2016. "Non-Newtonian versus numerical rheology: Practical impact of shear-thinning on the prediction of stable and unstable flows in intracranial anuerysms", *International Journal for Numerical Methods in Biomedical Engineering*, Vol. 33, Issue 7, e2836.

Lantz, J., and Renner, J., and Karlsson, M., 2011, "Wall shear stress in a subject specific human aorta - Influence of fluid-structure interaction", *International Journal of Applied Mechanics*, Vol. 4, pp 759-778.

Liberthson, R., and Pennington, D., and Jacobs, M., and Daggett, W., 1979. "Coarctation of the aorta: Review of 234 patients and clarification of management problems", *The American Journal of Cardiology*. Vol. 43, Issue 4, pp 835-840.

Long, J., and Undar, A., and Manning, KB., and Deutsch, S., 2005. "Viscoelasticity of pediatric blood and its implications for the testing of a pulsatile pediatric blood pump", *American Society for Artificial Internal Organs*. Vol. 51, Issue 5, pp 563-566.

Maivè, M., and Garcia, A., and Ohayon, J., and Martinez, M., 2012. "Unsteady blood flow and mass transfer of a human left coronary artery bifurcation: FSI vs. CFD", *International Coomunications in Heat and Mass Transfer.* Vol. 39, Issue 6, pp 745-751.

Olufsen, M., and S. Peskin, C., and Kim, W., and Pedersen, E., and Nadim, A., and Larsen, J., 2000. "Numerical Simulation and Experimental Validation of Blood Flow in Arteries with Structured-Tree Outflow Conditions", *Annals of Biomedical Engineering*. Vol. 28, pp 1281-1299.

Razavi, A., and Shirani, E., and Sadeghi M.R., 2011. "Numerical simulation of blood pulsatile flow in a stenosed carotid artery using different rheological models", *Journal of Biomechanics*,. Vol. 44, Issue 11, pp 2021-2030.

Song, X., and Wood, H., and Day, S., and Olsen, D., 2003. "Studies of Turbulence Models in a Computational Fluid Dynamics Model of a Blood Pump", *Artificial Organs*, Vol. 27, Issue 10, pp 935-937.

Soudah, E., and Oñate, E., and Cervera, M., 2016. "Computational Fluid Dynamics Indicators to Improve Cardiovascular Pathologies Diagnosis". *Monograph CIMNE.* M167.

Stein, PD., and Sabbah, Hn., 1976. "Turbulent blood flow in the ascending aorta of humans with normal and diseased aortic valves". *Circulation Research.* Vol. 39, pp 58-65.

Tukovic, Z., and Cardiff, P., and Karac, A., and Jasak, H., and Ivakovic, A, 2014. "OpenFOAM Library for Fluid Structure Interaction, *Technical Report 9th OpenFOAM Workshop*. Zagreb, Croatia.

Vignon-Clementel, I., and Figueroa, C., and Jansen, K., and Taylor, C., 2006. "Outflow boundary conditions for three-dimensional finite element modelling of blood flow and perssure in arteries", *Computer Methods in Applied Mechanics and Engineering*, Vol. 195, pp 3776-3796.

Vita, F., and Tullio, M., and Verzicco, R., 2015. "Numerical simulation of the non-Newtonian blood flow through a mechanical aortic valve", *Theoretical and Computational Fluid Dynamics*, Vol. 30, Issue 1-2, pp 129-138.

Vitanova, K., and Cleuziou, J., and Pabst, J., and Burri, M., and Eicken, A., and Lange, R., 2017, "Recoarctation After Norwood I Procedure for Hypoplastic Left Heart Syndrome: Impact of Patch Material", *Ann Thorac Surg*, Vol. 103, pp 617-621.

Ward, C., 2000. "Clinical significance of the bicuspid aortic valve", *Heart*, Vol. 83, pp 81-85.

Zhang, J., and Zhang, P., and Fraser, K., and Griffith, B., and Wu, Z., 2013. "Comparison of fluid dynamic numerical models for a clinical ventricular assist device and experimental validation", *Artificial Organ*,. Vol. 37, Issue 119, pp 380-389.